Computer Graphics Forum Vol 12 (3),
Proceedings of the EUROGRAPHICS '93,
Barcelona, Spain, Sept. 1993.

Automatic Reconstruction of Buildings from Stereoscopic Image Sequences

Reinhard Koch

Institut für Theoretische Nachrichtentechnik und Informationsverarbeitung
Universität Hannover, Appelstrasse 9A, 3000 Hannover 1, Germany
email: koch@tnt.uni–hannover.de

A vision–based 3–D scene analysis system is described that is capable to model complex real–world scenes like streets and buildings automatically from stereoscopic image pairs. Input to the system is a sequence of stereoscopic images taken with two standard CCD Cameras and TV lenses. The relative orientation of both cameras to each other is known by calibration. The camera pair is then moved throughout the scene and a long sequence of closely spaced views is recorded. Each of the stereoscopic image pairs is rectified and a dense map of 3–D surface points is obtained by area correlation, object segmentation, interpolation, and triangulation. 3–D camera motion relative to the scene coordinate system is tracked directly from the image sequence which allows to fuse 3–D surface measurements from different viewpoints into a consistent 3–D model scene. The surface geometry of each scene object is approximated by a triangular surface mesh which stores the surface texture in a texture map. From the textured 3–D models, realistic looking image sequences from arbitrary view points can be synthesized using computer graphics.

Key Words: Image Processing, Virtual Reality, 3–D Scene Analysis, Stereoscopic Image Sequence Analysis, Robot Vision, Scene Reconstruction, Close Range Photogrammetry.

1 Introduction

The rapid progress in the development of powerful computer graphics hardware and software enables users in a wide range of applications to gain a better insight into processes by visual simulation. Suppliers of flight and driving simulators as well as landscape and city planners are interested to simulate photo–realistic views of the environment. Architects and city planners for example construct new buildings with CAD systems and are interested to visualize their impact onto the existing environment beforehand. Complete realism, however, is possible only if the buildings to be constructed are placed inside a 3–D reconstruction of of the real environment. It is therefore necessary to reconstruct the existing environment as a 3–D model of the real scene with as little effort as possible [1]. One possible approach is to obtain a complete 3–D scene description by evaluating images of the scene.

Modeling of 3–D scenes from 2D image sequences has been a research topic for a long time as Aggarwal and Nandhakumar [2] showed in their overview of this field. The goal of such modeling is to extract a compact description of the scene for purposes of reconstruction [3], recognition [4], or data compression [5], [6]. When analyzing complex scenes with multiple moving flexible objects a complete description of all properties of the scene is necessary. In previous works the different properties 3–D object shape, 3–D object motion, and object surface texture were treated separately. Great effort went into developing algorithms that estimate 3–D object shape from various sources, termed shape from motion, stereo, texture, and others. [7]–[9]. On the other hand research was conducted to find solutions to the problem of rigid object motion [10], [11]. Only recently the problem of dynamic nonrigid bodies and nonrigid motion was addressed [12], [13].

Researchers are often just interested in some part of the 3–D scene information. Very precise geometric measurements of buildings like houses and bridges are performed in close range photogrammetry. Goal is the survey of

dynamic deformations in the structure of buildings or the recording of historical buildings where no drawings exists. The tool to obtain such precise 3–D measurement is usually a bundle block adjustment, where many photographs of the object are taken from different view points and selected image features together with some prior measured 3–D object coordinates are evaluated. For this procedure a high degree of manual interaction is still needed [14].

A qualitative geometric scene description is sufficient when constructing path planners for autonomous vehicles and robots. For that purpose obstacle maps are needed to avoid collisions and the precise geometry is of no interest. More important in this task is the fast and precise position estimation of the robot in the environment. For this approach usually image features like edges are selected automatically and tracked throughout the sequence. Monocular as well as stereoscopic sensors are used in this task [15].

An important scene property needed for visualization is the photometric surface description. People in the field of image communication, multi media, flight and driving simulation, and virtual reality demand the construction of complete realistic environments. Sometimes it is even more important to have a good surface texture description than to obtain a refined 3–D geometry. Texture maps that store real views of the object appearance can be used for that purpose [16].

The simultaneous estimation of object geometry and camera position is usually ill–posed because for the estimation of object geometry from different camera view points the camera position need to be known and vice versa. An interesting approach to overcome this difficulty was published by Tomasi and Kanade [17], who separate object geometry and camera motion information from a monocular image sequence. However, they assume an orthographic projection which requires the objects to be far away from the camera with a small viewing angle.

Automatic evaluation of all scene properties, camera position and 3–D object geometry as well as photometric surface mapping, for the purpose to reconstruct 3–D scene models for visualization, are discussed in this contribution. To overcome the problem of simultaneous estimation of object geometry and camera position, a calibrated stereoscopic image sequence is recorded. From each image pair the geometry is measured and from the sequence information relative camera motion can be extracted. All measurements obtained from the image sequence need then to be integrated into a consistent 3–D scene model that contains not only the scene geometry but also texture maps of the object surface. Visual simulations of the scene from this complete scene model can be performed with computer graphics.

The paper is organized as follows. Chapter 2 discusses the concept of the scene analysis system. Chapter 3 treats the measurement of object geometry from a single image pair whereas in Chapter 4 motion estimation and sequence accumulation is discussed. Chapter 5 concludes with some results of scene reconstruction.

2 Concept of 3–D Scene Analysis System

The structure of the scene analysis process is shown in Fig. 1. Four main modules (image analysis pipeline, control interface, motion compensated prediction, and 3–D model storage) can be identified. In the center there is the image analysis pipeline that computes a model scene M_k from a stereoscopic image pair L_k, R_k at time instant k and from the accumulated sequence information contained in the model storage M_{k-1}. Sequence information is included into the analysis pipeline by motion compensated prediction at all stages. The scene model M_{k-1} is transformed from frame k–1 into the current camera position at frame k by compensation of the camera motion. From the transformed model the predictions of disparity, segmentation, and object geometry are computed and merged with the new measurements to yield a depth map of the new scene model M_k.

In order to obtain an efficient 3–D surface description and to treat hidden surfaces properly, the depth map is converted into a triangular surface mesh. In addition, the surface texture for each triangular surface patch, which represents the photometric information, is stored in M_k. From the geometric and photometric information realistic looking image sequences I^*_k can be synthesized.

The analysis pipeline is controlled by a user interface, which takes commands from the operator and supplies the analysis procedures with the proper parameters. This interface allows to insert prior scene knowledge into the

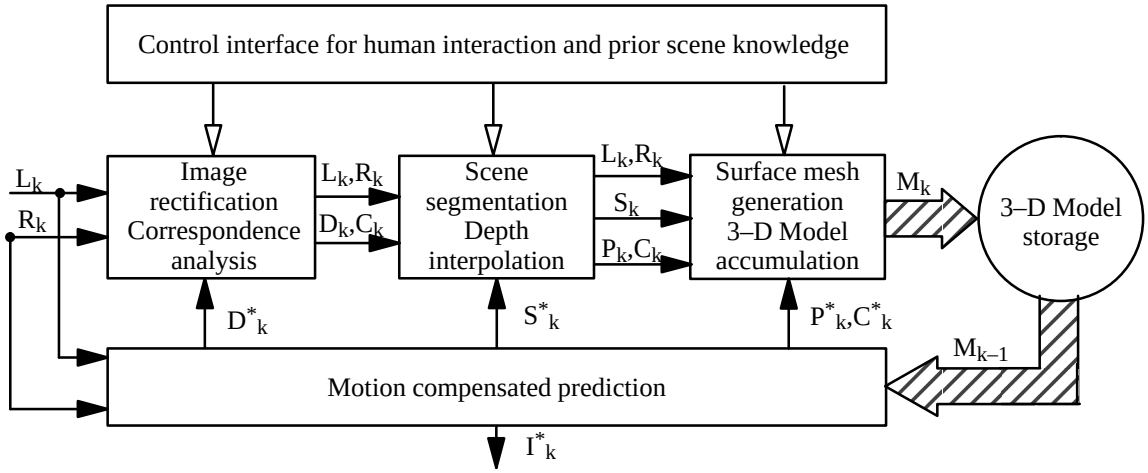

L_k: Left image D_k: Disparity map S_k: Segmentation map M_k: 3–D Scene model

R_k: Right image C_k: Confidence map P_k: Depth map

k: Index indicating the present time instant $*_k$: = data predicted from model M_{k-1} using motion compensation

I^*_k: Virtual camera image from model

Fig.1: Structure of 3–D Scene Analysis from Sequences of Stereo Images

analysis process. It is planned that this control interface will be replaced by a knowledge based system that automatically adapts the analysis parameters based on high level scene knowledge.

In the following sections the procedures for the image analysis pipeline and the 3–D motion compensated prediction are explained in more detail.

3 The Image Analysis Pipeline

The analysis of a stereoscopic image pair is split into correspondence analysis and object generation. Correspondence analysis tries to locally estimate image plane correspondences while during object generation areas in the image that belong to physically connected regions are merged by similarity measures. Each region is interpolated to yield a dense depth map and the measurements are triangulated and transformed into object space.

3.1 Correspondence analysis

The input to the system at time instant k is a stereo pair L_k, R_k. In a preprocessing step the stereoscopic camera is calibrated and each image pair is rectified to obtain an image pair where the camera axes are parallel and both cameras are displaced along horizontal image plane coordinates only. The calibration estimates radial lens distortion and the external orientation parameters of both cameras from a calibration pattern using a bundle block adjustment [18]. A projective transformation can be computed from the calibration parameters that warps the images to standard geometry. This image rectification greatly simplifies correspondence analysis and the search space is reduced to parallel horizontal epipolar lines **E**.

From the rectified images a disparity map D_k is obtained by correlation matching techniques. The quality of the match and therefore the quality of each displacement value is recorded in a confidence map C_k.The correspondence analysis is split into three parts. First a candidate for a corresponding point is identified in one image, then the corresponding candidate in the other image is searched for along the epipolar lines **E** and third the most probable candidate match between both images is selected based on a quality criteria. This search is repeated for each candidate, that is for each pixel. To select candidates the image grey level gradient **g** is evaluated. The image gradient is a vector field pointing into the direction of changing image texture like grey level edges. Only areas exceeding a minimum image gradient value $|\mathbf{g}| > g_{min}$ can be candidates for correspondence. The quality of the candidate can be estimated when comparing the gradient direction with the search direction. Edges perpendicular

a) left original image

b) right original image

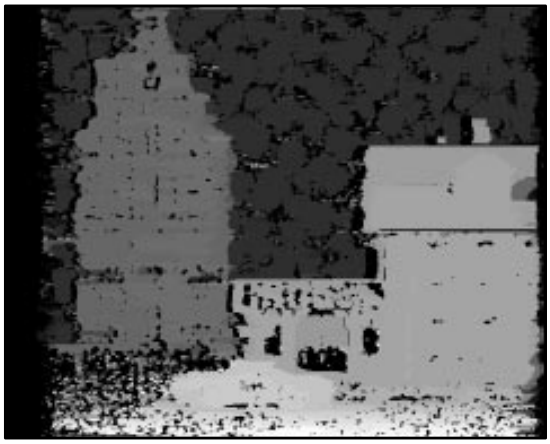

c) disparity map (dark = far from camera, light = near to camera, black = undefinded regions)

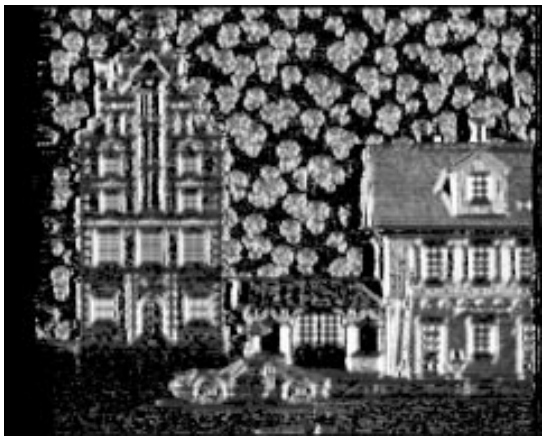

d) confidence map of disparity measurement (dark = low confidence, light = high confidence)

Fig. 2: Stereoscopic disparity analysis of image pair ”street”.

to the search direction can be located best while edges parallel to the search direction cannot be located at all. This quality measure C_1 can be calculated in Eq. (1). Candidates with $C_1 = 0$ can not be estimated while candidates with $C_1 = 1$ have highest confidence in estimation.

The estimation of C_1 is carried out for each image pixel. Each pixel with a gradient quality measure of $C_1 > 0$ will be selected as candidate. For each candidate a small measurement window (typically 7*7 pixel) around the candidate position in one grey level image is chosen and the corresponding grey level distribution is searched for in the other image. The search space is reduced to a one–dimensional search along the epipolar line between minimum and maximum disparity values derived from the known minimum and maximum scene distance. The search space may be extended to +/– 1 horizontal lines to account for calibration inaccuracies. The normalized cross correlation (NCC) is calculated between the candidates to select the most probable corresponding candidate along the search line. The most probable candidate pair is the pair with maximum cross correlation.

In complex scenes there may be multiple maxima or false maxima in the search space due to occlusions, repeated structures or image noise. This ambiguity can be reduced when uniqueness and ordering constraints are exploited. These constraints are based on the fact that there can be no more than one match between left and right image points and that matches are in order for physical surfaces [19]. These constraints are employed in an optimum search procedure using dynamic programming that matches all correspondences between left and right image that lie on

the same epipolar line. The dynamic programming algorithm was adapted from the work of Cox et al. [20]. The disparity value obtained for each candidate is recorded in a disparity map.

The NCC is additionally used to define the correspondence quality. Selected corresponding pairs with low NCC are corresponding points with low confidence. Therefore a second quality measure C_2 in Eq. (1) can be defined that reflects the correspondence measurement confidence. Experiments have shown that candidates below a minimum threshold NCC_{min} (NCC_{min} being approximately 0.5) are most often false matches that should be discarded. The confidence quality is therefore defined to be zero below NCC_{min} and NCC elsewhere.

$$C_1 = \left\{ \begin{array}{ll} 0 & \text{for } |\mathbf{g}| < g_{min} \\ \dfrac{\mathbf{g} \cdot \mathbf{E}}{|\mathbf{g}|} & \text{else} \end{array} \right\}, \quad C_2 = \left\{ \begin{array}{ll} 0 & \text{for NCC} < NCC_{min} \\ \text{NCC} & \text{else} \end{array} \right\} \tag{1}$$

Both quality measures can be merged to one measure $C_c = C_1 \cdot C_2$ with $\{0 \leq C_c < 1\}$ that contains the combined quality measure for each candidate. The confidence measure C_c is recorded for each candidate pixel in a confidence map. Fig. 2 demonstrates the correspondence analysis for the image pair "street". Disparity values between 10 and 50 pixel were measured. Fig. 2a and b show the left and right input image and Fig. 2c the measured disparity map with corresponding confidence map in Fig. 2d. Light grey levels in Fig. 2c show large disparities (foreground) and dark grey levels indicate small disparities (background). Light values in the confidence image indicate high, dark values low measurement confidence. Black regions are regions where the confidence measure is zero and where no measurement was possible.

3.2 Scene segmentation, Interpolation and Triangulation

The correspondence analysis yields a disparity map based on local depth measurement only. These measurements are corrupted by noise and must be merged to regions that describe physical object surfaces. Based on similarity measures the segmentation divides the viewed scene into object surfaces. As similarity measure the estimated disparities as well as grey level statistics are used to group pixels into object regions. The region boundaries are then corrected from the grey level image with a contour approximation by assuming that physical object boundaries most often create grey level edges in the image. The object segmentation for the image pair "street" is shown in Fig. 3a with each object having a distinct label marked as grey level in the map. The segmentation areas correspond to the background (label 1,2), the two houses (label 3,4), the car (5) and a foreground area (6).

The image segmentation is no trivial task and we are still working to improve it. One extension will be to consider regions of similar surface orientation, rather than just similar depth, as object surfaces. Another issue is the detection of surface creases at object corners in addition to depth continuities. For this task we are employing specific prior scene knowledge of object geometry.

Disparity Interpolation

The disparity measurements are noisy and there exist gaps in the surface that need to be filled. Once the disparity map is segmented into object regions all measurements of one region are interpolated by a thin plate surface model that calculates the best quadratic surface approximation of the disparity map based on the uncertain depth measures. Each disparity measurement has an uncertainty attributed to it which serves as a weight of the measurement. A multi grid surface reconstruction algorithm described by Terzopoulos [21] was chosen to calculate the interpolation with a finite element approximation. It is assumed that each segmented area contains a smooth coherent surface that can be modeled as a thin plate with a certain stiffness and that inside such a region the disparity measurements are corrupted by noise. The physical model of a thin plate can be formulated as a variational functional of the Euler–Lagrange equation $\Delta^2 d_{(x,y)} = 0$ with additional constraints at the boundaries. The interpolation solves the problem of minimizing the potential energy function of the thin plate that is deformed by the disparity measurements.

The solution to the energy minimization is obtained as a finite element approximation (FEM) as defined by Terzopoulos. As the basic element a quadratic patch with the size of the image pixel grid is used. A free boundary is defined at the edges of the segmentation area. Computation is simplified by the definition of 'computational

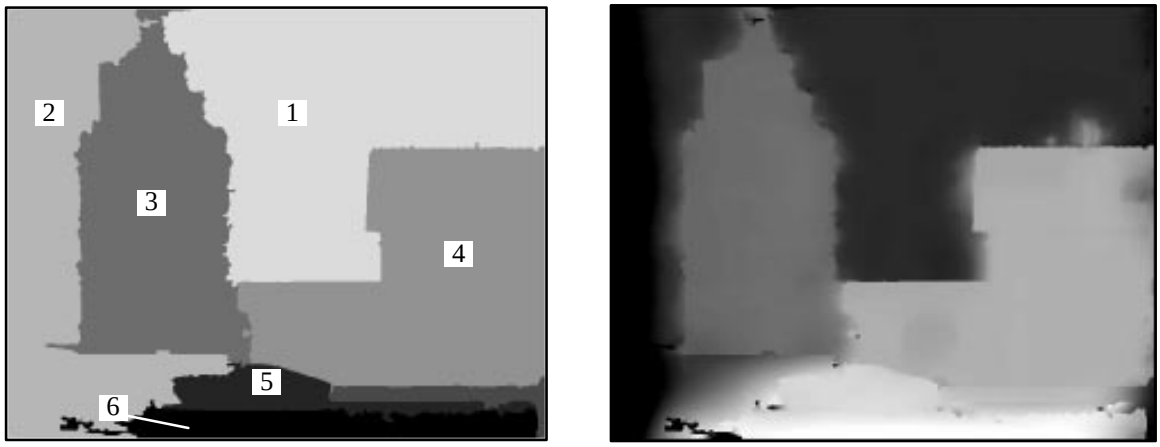

a) object segmentation map, each grey level labels one object surface

b) Thin plate interpolation of disparity map (dark = far from camera, light = near to camera)

Fig. 3: Segmentation and interpolation of image pair ”street”.

molecules' that define the local energy for each grid point. Inside of the thin plate, each grid point is affected by at most 12 neighboring grid points. At the plate boundary, only existing grid points contribute to the local energy function of that point. The local energy function for each grid point is accumulated and the energy functional for each segmented area is solved by Gauss–Seidel–Iteration.

The number of grid points equal the total number of pixel in the image. Solving of such a big equation system (with up to 720x576 equations for CCIR images) directly is prohibitive. To speed up computation, a multi grid technique with a 5 level image pyramid was implemented. The interpolation starts at the lowest level which in turn is used as starting value for the next higher level. With this approach, a CCIR size image is interpolated in about 5 –10 minutes on a SUN SPARCStation 10. The result of the disparity interpolation is shown in Fig. 3b for the scene ”street”. From the discrete and noisy disparity measurements in Fig. 2c together with the associated confidence values in Fig. 2d and the object segmentation from Fig. 3a, a continuous and dense disparity interpolation for each segmented region was performed that filled the gaps and smoothed the disparity estimates. Disparity discontinuities are preserved at the segmentation boundaries.

Triangulation

The interpolated depth map contains the visible scene geometry measured from a single camera view point. Whenever the scene contains occluded surfaces then the camera must be moved around the objects and the measurements from multiple view points must be included. For that purpose the 2D depth map is first converted into a 3–D surface description that can be modified to include hidden surfaces. The transformation is very simple because the images are rectified and relative 3–D–coordinates are obtained relative to the left camera center. The camera centers are displaced by the basis b in x–direction and both cameras have the same focal length f. In this case the relative object coordinate $\mathbf{P}_{(x,y)}$ for each pixel (x, y) in the left image with corresponding disparity value d(x, y) is recorded in a depth map $\mathbf{P}_k$.

$$\mathbf{P}_{(x,y)} = (P_x P_y P_z)^T = \frac{b}{d_{(x,y)}} \cdot (x, y, f)^T \qquad (2)$$

The depth map can be converted into a piecewise continuous, parametric 3–D surface description by spanning a wireframe in space for each segmented object surface. For each object region the depth map is approximated by triangular, planar surface patches. The triangular mesh was chosen because it is capable to approximate arbitrary surface geometries without singularities. On the surface of each triangular patch the object surface texture is stored in a texture map from which a naturally looking view of the original objects can be synthesized with texture mapping. In Fig. 4a the generation of the wireframe for the dominant objects in the scene ”street” are shown. For each triangular patch the corresponding image texture is stored and used to synthesize computer generated views

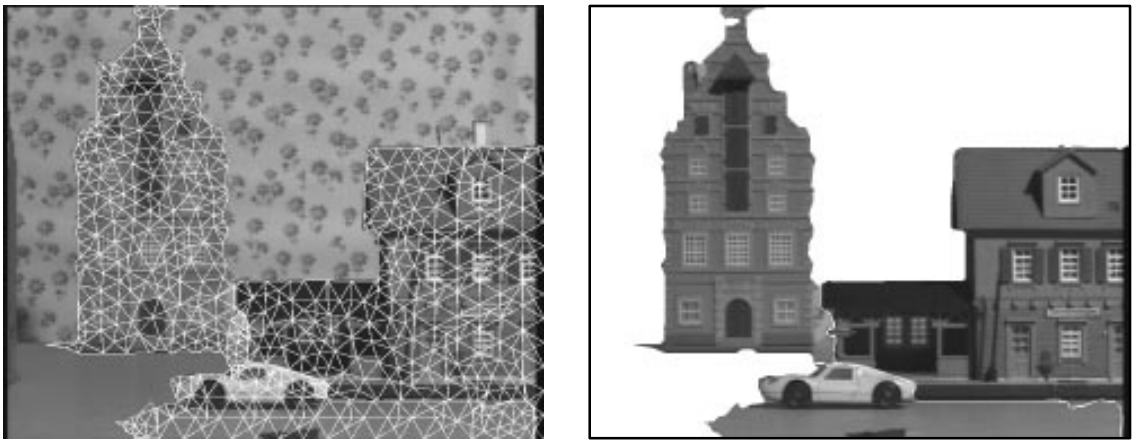

a) Triangular surface mesh of the main scene objects, superimposed onto the left image

b) synthesis of the main scene objects from the 3–D surface model

Fig. 4: Triangulation and model buildung.

which is shown in Fig. 4b. The surface geometry was calculated from the interpolated disparity map while the surface texture was taken from the left original image.

4 3–D motion compensated prediction

The tasks performed so far were straight forward stereoscopic image analysis. From a stereoscopic image pair a 3–D surface approximation was extracted from a single camera view point together with a quality measure of the estimated surface position. When complex scenes with occluding objects are analyzed then measurements from multiple view points have to be integrated into the 3–D surface model. Therefore it is necessary to estimate the 3–D motion of the camera and possible object motions in the scene from the image sequence and to fuse the multiple depth measurements into a consistent 3–D scene model.

4.1 3–D motion estimation using analysis by synthesis

In this section an algorithm to directly estimate 3–D scene motion from a monocular or stereoscopic image sequence is described shortly. A complete discussion of the algorithm can be found in [22]–[24].

An object is defined as a rigid 3–D–surface in space that is spanned by a set of N control points. A set of six motion parameters is associated with each object. Object motion is defined as rotation of the object control points around the object center followed by a translation of the object center, measured between two successive image frames k–1 and k. The object center **G** is the mean position vector of all N object control points. Each object control point $\mathbf{P_{i(k-1)}}$ at frame k–1 is transformed to its new position $\mathbf{P_{i(k)}}$ in frame k according to the general motion Eq. (3) between frame k–1 and k.

$$\mathbf{P_{i(k)}} = [\mathbf{R_G}] \cdot (\mathbf{P_{i(k-1)}} - \mathbf{G}) + \mathbf{G} + \mathbf{T} \tag{3}$$

with $\mathbf{T} = (T_x, T_y, T_z)^T =$ translation vector, $\mathbf{G} = (G_x, G_y, G_z)^T = \sum_{i=1}^{N} \frac{\mathbf{P_i}}{N} =$ component center, and

$[\mathbf{R_G}] =$ matrix of rotation vector $\mathbf{R} = (R_x, R_y, R_z)^T$

Object rotation can be expressed by a rotation vector $\mathbf{R} = (R_x, R_y, R_z)^T$ that describes the successive rotation of the object around the three axes $(x, y, z)^T$ parallel to the scene coordinate system centered at **G**. From this vector the rotation matrix $[\mathbf{R_G}]$ is derived when the identical matrix [**I**] is rotated around the coordinate axes with R_x first, R_y second and R_z last. Because $[\mathbf{R_G}]$ is derived from the rotation vector **R**, the six parameters of **T** and **R** suffice to describe the 3–D object motion.

The only information available to the analysis system is the surface texture projected onto the camera target throughout the image sequence. From this sequence the motion parameters have to be derived. Assume a scene with an arbitrarily shaped, moving textured object observed by a camera during frames k–1 and k. The object moves between frame k–1 and k according to the general motion Eq. (3) with motion parameters **R** and **T**. A point on the object surface, called observation point $\mathbf{P}_{(k-1)}$, holds the surface intensity I_1, which is projected onto $\mathbf{p}_1$ in the image plane at frame k–1. At frame k $\mathbf{P}_{(k-1)}$ is moved to $\mathbf{P}_{(k)}$, still holding I_1 that is now projected onto $\mathbf{p}_2$. In image frame k the surface intensity I_1 will now be projected at image position $\mathbf{p}_2$, whereas the image intensity at point $\mathbf{p}_1$ has changed to I_2.

The image displacement vector $\mathbf{d} = \mathbf{p}_2 - \mathbf{p}_1$ is called optical flow vector and describes the projection of the observation point displacement $\mathbf{P}_{(k)} - \mathbf{P}_{(k-1)}$ onto the image plane. When assuming a linear dependency of the surface texture between I_1 and I_2 and a brightness constancy constraint between frame k–1 and k it is possible to predict I_2 from I_1 and its corresponding image intensity gradients and hence to estimate **d** from the measurable difference $I_2 - I_1$. I_2 is measured at position of $\mathbf{p}_1$ at frame k, where I_1 is taken from image position $\mathbf{p}_1$ at frame k–1. When approximating the spatial derivatives as finite differences the optical flow vector $\mathbf{d} = (d_x, d_y)^T$ can be predicted from the image gradients $\mathbf{g} = (g_x, g_y)^T$ and the temporal image intensity difference $\Delta I_{\mathbf{p1}} = I_2 - I_1$ between frame k and k–1 at $\mathbf{p}_1$ in Eq. (4):

$$\Delta I_{\mathbf{p1}} \;=\; \mathbf{g} \cdot \mathbf{d} \;=\; g_x \cdot d_x + g_y \cdot d_y \;=\; g_x \cdot (p_{2x} - p_{1x}) + g_y \cdot (p_{2y} - p_{1y}) \tag{4}$$

In Eq. (4) **d** is related to intensity differences. Substituting the perspective projection of $\mathbf{P}_{(k-1)}$ and $\mathbf{P}_{(k)}$ for $\mathbf{p}_1$ and $\mathbf{p}_2$ in Eq. (4) yields a direct geometric to photometric transform that relates the spatial movement of **P** between frame k–1 and k to temporal intensity changes in the image sequence at $\mathbf{p}_1$.

$$\Delta I_{\mathbf{p1}} \;=\; f \cdot g_x \cdot \left(\frac{P_{(k)x}}{P_{(k)z}} - \frac{P_{(k-1)x}}{P_{(k-1)z}} \right) + \; f \cdot g_y \cdot \left(\frac{P_{(k)y}}{P_{(k)z}} - \frac{P_{(k-1)y}}{P_{(k-1)z}} \right) \tag{5}$$

With this approach, rigid 3–D object motion can be estimated directly from the image sequence when the object shape $\mathbf{P}_{(k-1)}$ is known. Assuming that rotation between successive images is small, $[\mathbf{R_G}]$ can be linearized and $\mathbf{P}_{(k)}$ is substituted in Eq. (5) as a function of the unknown parameter **R** and **T** as derived in Eq. (3) :

$$\begin{aligned}
\Delta I_{p1} \cdot P_z^2 \;=\;& f \cdot g_x \cdot P_z \cdot \mathbf{T_x} + f \cdot g_y \cdot P_z \cdot \mathbf{T_y} - [\, \Delta I_{p1} \cdot P_z + f \cdot P_x g_x + f \cdot P_y g_y \,] \cdot \mathbf{T_z} \\
&- [\, \Delta I_{p1} \cdot P_z \cdot (P_y - G_y) + f \cdot P_x \cdot g_x \cdot (P_y - G_y) + f \cdot P_y \cdot g_y \cdot (P_y - G_y) + f \cdot P_z \cdot g_y \cdot (P_z - G_z) \,] \cdot \mathbf{R_x} \\
&+ [\, \Delta I_{p1} \cdot P_z \cdot (P_x - G_x) + f \cdot P_x \cdot g_x \cdot (P_x - G_x) + f \cdot P_y \cdot g_y \cdot (P_x - G_x) + f \cdot P_z \cdot g_x \cdot (P_z - G_z) \,] \cdot \mathbf{R_y} \\
&+ [\, f \cdot P_x \cdot g_y \cdot (P_x - G_x) - f \cdot P_z \cdot g_x \cdot (P_y - G_y) \,] \cdot \mathbf{R_z}
\end{aligned}$$

with $(P_x, P_y, P_z)^T = \mathbf{P}_{(k-1)}$. (6)

For 3–D motion estimation the object shape is assumed to be known. An initial estimate of the scene shape was generated from stereoscopic image analysis. When the initial estimate fails this dependency may affect the analysis and will sometimes lead to estimation errors. As long as the initial shape approximation is reliable, however, this dependency can be neglected. When a stereoscopic image sequence is available, then both images of the pair can be used to further improve the motion estimation. The left image coordinate system is used as reference system and measurements are taken from the left camera as before in Eq. (6). Measurements taken from the right camera will be transformed according to Eq. (7), where an observation point $\mathbf{P}_{R(k)}$ is expressed relative to the left camera coordinate system.

$$\begin{aligned}
\mathbf{P}_{R(k)} \;&=\; [\mathbf{R_{LR}}] \cdot \mathbf{P}_{L(k)} + \mathbf{T}_{LR} \\
&=\; [\mathbf{R_{LR}}] \cdot \left([\mathbf{R_G}] \cdot (\mathbf{P}_{L(k-1)} - \mathbf{G}_{L(k-1)}) + \mathbf{T} + \mathbf{G}_{L(k-1)} \right) + \mathbf{T}_{LR} \\
&=\; [\mathbf{R_{LR}}] \cdot [\mathbf{R_G}] \cdot \left(\mathbf{P}_{L(k-1)} - \mathbf{G}_{L(k-1)} \right) + [\mathbf{R_{LR}}] \cdot \left(\mathbf{T} + \mathbf{G}_{L(k-1)} \right) + \mathbf{T}_{LR}
\end{aligned} \tag{7}$$

with: $[\mathbf{R_{LR}}], \mathbf{T}_{LR}$ = Transformation from left to right camera coordinate system

The Transformation ($[\mathbf{R}_{LR}]$, $\mathbf{T}_{LR}$) is known from calibration and is particularly easy for rectified images. The motion Eq. (7) for the right image can be inserted in Eq. (5) as before and the measurement equation for the right image is derived which doubles the number of independent measurements for motion estimation.

Conditions for robust motion estimation

At least six distinctive observation points that lead to six linear independent equations are needed to solve for the six motion parameters **R** and **T**. In real imaging situations the measurements of the spatial and temporal derivatives are noisy and some of the observation points selected may be linear dependent of each other. To cope with those conditions more than six observations are evaluated and a linear regression is carried out using least squares fit. As observation points all surface points with a gradient exceeding a noise threshold can be used. To avoid linear dependencies of the measurement equations, the observation points should be evenly distributed across the object surface. Based on that rule, typically 100 to 1000 surface points are selected as observation points. All observation points of one object are evaluated. It is important to note that we do **not** measure optical flow locally and then try to combine the flow field. Instead **all** observation points of a rigid surface are used to solve for **R** and **T**. To account for the linearizing of $[\mathbf{R}_G]$ and nonlinear grey level distribution, the estimation is iterated. The position **P** of each observation point is initially determined by object shape and position. An estimate of the parameters **R** and **T** is calculated and the observation point is moved according to those parameters. The estimation is repeated with the new starting position of **P** until the parameter changes of **T** and **R** converge to zero.

4.2 Accumulation of multiple depth maps into a common 3–D scene model

For each image pair of the sequence a depth map D_k was calculated by stereoscopic analysis together with its associated confidence map C_k. 3–D camera motion between successive frames was estimated which allows to register the image pairs relative to another. The goal of sequence accumulation is to fuse the depth measurements from the image sequence into a consistent 3–D scene model to improve estimation quality. Consistency is achieved by compensating the camera motion from frame k–1 to k. The scene model is transformed into frame k with the estimated motion parameters. From the model geometry in this position a prediction of the disparity map d^*_k can be computed and compared with the measured disparity map d_k to detect geometric errors.

Two types of geometric errors can be identified: Gross errors where the disparity estimation failed due to occlusions, repeated structures, or noise; and quantization errors due to the limited resolution of the disparity d. Gross errors can be detected and excluded from the analysis by comparing the predicted disparity map d^*_k with the measured disparity map at frame k. In areas of large disparity difference only the measurement with higher confidence C_c should be chosen. The quantization of d leads to a quantization in depth estimation according to Eq. (2) which can be severe for a small base line b between the cameras and coarse resolution of d. The quantization of d is determined by the stereoscopic analysis process itself and cannot be improved. Moving the camera, however, is equivalent to increasing the base line b and hence increasing depth resolution.

In this approach the depth measurements are improved by weighted depth accumulation from the motion compensated sequence of depth maps. For each observation point **P** of the surface there exist a confidence value C_c from Eq. (1) that expresses the measurement accuracy. The confidence value C_c is converted into the weight S according to Eq. (8) that can easily be accumulated throughout the sequence. Each observation point holds not only its position $\mathbf{P}_{k-1}$ in space but also its corresponding confidence weight $S_{k-1} = S^*_k$. $\mathbf{P}_{k-1}$ is transformed to $\mathbf{P}^*_k$ according to Eq. (3) and its projection (x,y) in the image is computed. The disparity d_k, measured in frame k at image position (x,y) with corresponding weight S_k, is converted to a depth measurement $\mathbf{P}_k$ and fused with $\mathbf{P}^*_k$ in a weighted accumulation to compute the improved depth estimate $\mathbf{P}_k$new and weight $S_k$new:

$$\mathbf{P}_k\text{new} = \frac{\mathbf{P}^*_k \cdot S^*_k + \mathbf{P}_k \cdot S_k}{S^*_k + S_k} \quad \text{and} \quad \begin{aligned} S_k\text{new} &= S^*_k + S_k \\ \text{with} \quad S &= \frac{C_c}{1 - C_c} \end{aligned} \tag{8}$$

The information fusing process described above can only be applied to an existing surface. When new objects and prior unseen object surfaces appear, the surface mesh must be extended from the new measurement. Once the surface is built, the fusing process can continue.

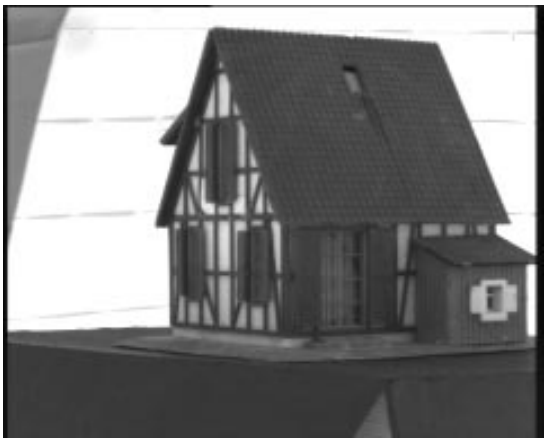

a) left original image of sequence ”house”

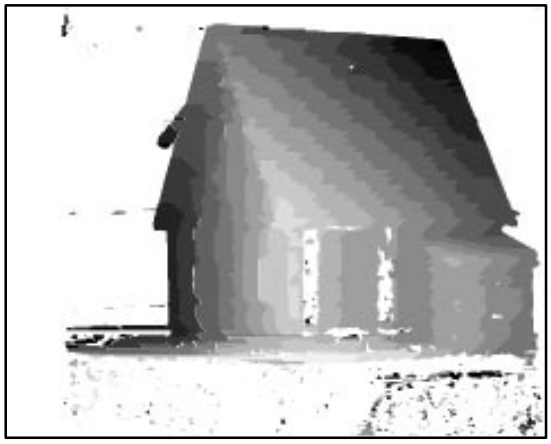

b) disparity map estimated from single image pair with 1 pixel resolution

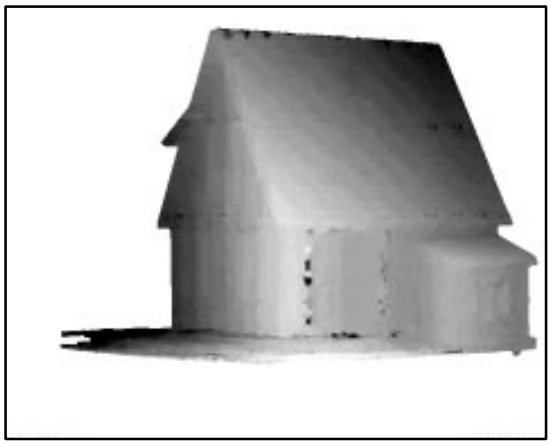

c) accumulated disparity map estimated from 9 adjacent image pairs, gaining sub pixel resolution

d) smooth disparity map interpolated from the accumulated disparity map in Fig. 5c

Fig. 5: Disparity accumulation for the sequence ”house”.

The results of the depth fusing process are shown in Fig. 5 for the sequence ”house”. A toy house was rotated on a turn table and 90 stereoscopic views of the house from all directions, each view displaced by 4 degree of rotation, were taken. In Fig. 5a the left original view of the house is shown. For each image pair a disparity map (Fig. 5b) was computed, a 3–D surface object was generated and the relative 3–D motion and rotation of the house was estimated successfully. To demonstrate the accumulation process, the disparity maps from 9 adjacent frames (center frame and 4 frames to each side) were fused into a combined depth map in Fig. 5c. Each disparity map was estimated with a disparity resolution of 1 pixel. The quantization effects are clearly visible in Fig. 5b. About 10 different depth values can be measured. In comparison to the single map an increase of resolution to sub pixel accuracy can be seen in Fig. 5c. This disparity map is further enhanced by interpolation to create the smooth disparity map as shown in Fig. 5d.

5 Conclusion and Results

A system for automatic 3–D scene analysis was discussed. The system is capable to analyze a complex real scene with multiple overlapping objects from an arbitrary moving stereoscopic video camera system. It segments the scene into smooth surfaces and stores the true 3–D geometry of the scene in a 3–D scene model, including surface texture. Camera motion is tracked throughout the sequence and measurements from different view points are integrated into the model data base.

Fig. 6: Synthesized view of the combined scene of 3–D models ”street” and ”house”.

The system implementation is not jet finished. With the current implementation, we are not able to add new scene contents (e.g. from moving around a corner of a house) automatically into the model to include truly occluded surfaces. We are further investigating the impact of erroneous model shape on the camera tracking algorithm and we are working to improve shape accumulation further through Kalman filtering. Some of the analysis parameters for disparity estimation, image segmentation, and surface mesh generation were chosen prior to the analysis process. An important additional step towards fully automated scene analysis will be the extension of the control interface with knowledge based scene interpretation, a project we are currently investigating.

Despite these problems the system is already capable to solve some important tasks. It was used for model–based data compression in stereoscopic television scenes, where it serves to generate a compact description of the 3–D scene viewed by a stereoscopic camera system. The 3–D model is transmitted once and from that on only camera motion and changing image content is updated. The receiver recovers the original image sequence by synthesizing the stereoscopic image sequence from the model scene [24].

Another application of the system is the visual reconstruction and modification of a real environment as motivated by architects and city planners. They are interested to change the existing environment and to place new buildings inside of an existing real scene. This application was simulated in Fig. 6, where the house and the street scene modeled before are merged into one scene. With the 3–D models of the scenes ”street” and ”house” available, new realistic views of a combined scene can be formed. Because the 3–D geometry of the objects is modeled, the house can be placed **inside** the street scene with proper 3–D depth scaling. The car which is in the foreground occludes the toy house while the toy house occludes the big house in the background.

Acknowledgement

This work has been supported by a grant of the German postal service TELEKOM.

References

[1] P. Durisch, "Photogrammetry and Computer Graphics for Visual Impact Analysis in Architecture", *ISPRS Conference 1992*, Vol. 29, B5, pp. 434–445, Washington, D.C. Aug. 1992.

[2] J.K. Aggarwal, N. Nandhakumar, "On the Computation of Motion from Sequences of Images –A Review," *Proc. of the IEEE*, Vol. 76 (8), pp. 917–935, Aug. 1988.

[3] A. Blake, A. Zissermann, "Visual Reconstruction," *MIT–Press*, Cambridge, 1987.

[4] D. Marr, K. H. Nishihara, "Representation and recognition of the spatial organization of threedimensional shapes," *Proc. Royal. Soc. Lond. B*, vol. 200, pp. 269 –294, 1978.

[5] H.G. Musmann, M. Hötter, J. Ostermann, "Object–oriented analysis–synthesis coding of moving images," *Signal Processing: Image Communication*, Vol. 1 (2), pp. 117–138, Nov. 1989.

[6] H. Harashima, F. Kishino, "Intelligent Image Coding and Communications with Realistic Sensations – Recent Trends,", *IEICE Transactions*, Vol. E 74 (6), pp. 1582–1592, June 1991.

[7] R. A. Jarvis, "A Perspective on Range Finding Techniques for Computer Vision," *IEEE Transactions on Pattern Analysis and Machine Intelligence*, Vol. 5 (2), pp. 122–139, March 1983.

[8] H.H. Baker, T.O. Binford: "Depth from edge and intensity based stereo," *Proc. seventh Int. joint Conf. Artif. Intell*. pp. 632–636, 1981.

[9] J. Aloimonos, D. Shulman, "Integration of Visual Modules," *Academic Press*, San Diego, USA, 1989.

[10] A.N. Netravali, J. Salz, "Algorithms for Estimation of Three–Dimensional Motion," *AT&T Technical Journal*, Vol. 64 (2), 1985.

[11] R.Y. Tsai, T.S. Huang, "Uniqueness and estimation of three–dimensional motion parameters of rigid objects with curved surfaces," *IEEE Transactions on Pattern Analysis and Machine Intelligence*, Vol 6 (1), pp. 13–26, 1984.

[12] D. Terzopoulos , D. Metaxas, "Dynamic 3D Models with Local and Global Deformations: Deformable superquadratics," *IEEE Transactions on Pattern Analysis and Machine Intelligence*, Vol. 13 (7), pp. 703–714, July 1991.

[13] A. Pentland, B. Horowitz, "Recovery of Nonrigid Motion and Structure," *IEEE Transactions on Pattern Analysis and Machine Intelligence*, Vol. 13 (7), pp. 730–742, July 1991.

[14] A. Streilein, H. Beyer, T. Kersten,"Digital Photogrammetric Techniques for Architectural Design", *ISPRS Conference 1992*, Vol. 29, B5, pp. 825–831, Washington, D.C. Aug. 1992.

[15] M. Buffa, O. Faugeras, Z. Zhang, "A Complete Navigation System for a Mobile Robot Using Real–time Stereovision and the Delauney Triangulation", *IAPR Workshop on Machine Vision Application*, Dec. 92, Tokyo

[16] Koch, R.,1990. Automatic Modelling of Natural Scenes for Generating Synthetic Movies, Eurographics '90, Montreux, Switzerland.

[17] C. Tomasi, T. Kanade,"Shape and Motion from Image Streams under Orthography: a Factorization Method", *Intl. Journal of Computer Graphics*, Vol. 9:2, pp. 137–154, 1992.

[18] K. Jacobson,"BUNOR – Stereoscopic bundle block adjustment program", Institut für Photogrammetrie und Ingenieurvermessung, Universität Hannover, 1992.

[19] Marr, D., 1982. Vision – A Computational Investigation into the Human Representation and Processing of Visual Information, W.H. Freeman & Co., New York, USA.

[20] Cox, I., Hingorani, S., Maggs, B., Rao, S.," Stereo without Regularisation", *British Machine Vision Conference*, Leeds, UK, pp. 337–346, David Hogg & Roger Boyle (ed.), Springer Verlag, 1992.

[21] Terzopoulos, D., 1988. The computation of visible–surface representations, IEEE Trans. Patt. Anal. Mach. Intell., Vol 10, pp.417–438.

[22] Kappei, F., 1988. Modellierung und Rekonstruktion bewegter dreidimensionaler Objekte aus einer Fernsehbildfolge, Ph.D. Thesis, University of Hannover.

[23] R. Koch,"Dynamic 3D Scene Analysis through Synthesis Feedback Control", *IEEE Trans. Patt. Anal. Mach. Intell., Special issue on analysis and synthesis*, Vol. 15:6, June 1993.

[24] L. Falkenhagen, D. Pele," Specification of Algorithm for Object Based 3D Motion Estimation", *RACE Project R2045/UH/DS/P/002/b1, DISTIMA*, Bruxelles, 1992.